International Journal of Nanomedicine

Dovepress
open access to scientific and medical research

Open Access Full Text Article

ORIGINAL RESEARCH

Ultrasmall superparamagnetic nanoparticles targeting E-selectin: synthesis and effects in mice in vitro and in vivo

This article was published in the following Dove Press journal:
International Journal of Nanomedicine

Lijuan Liu*
Lu Liu*
Yin Li
Xiaoxin Huang
Donglian Gu
Bo Wei
Danke Su
Guanqiao Jin

Centre of Imaging Diagnosis, Affiliated Tumor Hospital of Guangxi Medical University, Nanning, Guangxi, People's Republic of China

*These authors contributed equally to this work

Purpose: We developed a contrast agent for targeting E-selectin expression. We detected the agent using magnetic resonance imaging (MRI) in vivo in nude mice that had undergone nasopharyngeal carcinoma (NPC) metastasis.

Methods: Sialyl Lewis X (sLe^X) was conjugated with ultrasmall superparamagnetic iron oxide (USPIO) nanoparticles. Hydrodynamic size, polydispersity index, and ζ-potential of USPIO–polyethylene glycol (PEG) nanoparticles and USPIO-PEG-sLe^X nanoparticles were measured. Component changes in nanoparticles of USPIO, USPIO-PEG, and USPIO-PEG-sLe^X were analyzed by thermogravimetric analysis and Fourier-transform infrared spectroscopy. A model of NPC metastasis to inguinal lymph nodes in nude mice was used to investigate characteristics of the USPIO-PEG-sLe^X nanoparticles in vivo. We investigated the ability of the T2* value, change in T2* value (ΔT2* value), and enhancement rate (ER) to assess accumulation of USPIO-PEG-sLe^X nanoparticles quantitatively in mice of a metastasis group and control group. Four MRI scans were undertaken for each mouse. The first scan (t0) was done before administration of USPIO-PEG-sLe^X nanoparticles (0.1 mL) via the tail vein. The other scans were carried out at 0 (t1), 1 (t2), and 2 hours (t3) postinjection. The mean optical density was used to reflect E-selectin expression.

Results: sLe^X was labeled onto USPIO successfully. In vivo, there were significant interactions between the groups and time for T2* values after administration of USPIO-PEG-sLe^X nanoparticles. Six parameters (T2* at t2, ΔT2* at t1, ΔT2* at t2, ER at t1, ER at t2, and ER at t3) were correlated with the mean optical density.

Conclusion: USPIO-PEG-sLe^X nanoparticles can be used to assess E-selectin expression quantitatively. Use of such molecular probes could enable detection of early metastasis of NPC, more accurate staging, and treatment monitoring.

Keywords: molecular MRI, contrast agent, E-selectin, Sialyl Lewis X, nasopharyngeal carcinoma, iron oxide

Introduction

Nasopharyngeal carcinoma (NPC) may be considered one of the rarer forms of cancer worldwide, but it has high incidence in particular geographic and ethnic populations.[1,2] For instance, NPC incidence is high in southern China.[3]

NPC is characterized by a high degree of local invasion and early distant metastasis.[1] Also, 6%–15% of NPC patients have distant metastasis at initial diagnosis.[4] Distant metastasis is a leading cause of treatment failure for NPC.[5] In pretreatment evaluation of NPC, imaging methods that can depict metastatic lesions reliably are necessary, because imaging findings guide management.

Correspondence: Guanqiao Jin; Danke Su
Centre of Imaging Diagnosis, Affiliated Tumor Hospital of Guangxi Medical University, 71 Hedi Road, Nanning, Guangxi, People's Republic of China
Tel +86 134 8109 7306
Fax +86 771 530 8223
Email jinguanqiao77@gxmu.edu.cn; sudanke@gxmu.edu.cn

submit your manuscript | www.dovepress.com
DovePress
http://doi.org/10.2147/IJN.S199571

Several studies have shown high expression of E-selectin to be closely related to the metastasis of various malignant tumors.[6–11] E-selectin is also known as CD62E, ELAM1, or LECAM2.[12,13] E-selectin is a transmembrane protein containing lectin-like and EGF-like domains, followed by short cysteine-rich repeats.[14] The carbohydrate ligand of E-selectin is sialyl Lewis X (sLe^x).[15,16] E-selection and its ligands are important in the inflammatory response and cancer metastasis.[17–19] Our research team has shown that E-selectin has a critical role in NPC metastasis and represents an independent predictor of poor outcomes.[20] E-selectin can be used to label and track tumor cells.

Molecular imaging can be defined broadly as the in vivo characterization and measurement of biological processes at cellular and molecular levels.[21] Intracellular labeling has been used to track cells in vivo by employing magnetic resonance imaging (MRI).[22] MRI is the primary imaging method and diagnostic basis for T and N staging of NPC,[6] because of its excellent soft-tissue resolution and multiple-plane imaging.[23] Consequently, finding new MRI agents to diagnose NPC metastasis is important.

Ultrasmall superparamagnetic iron oxide (USPIO) nanoparticles are emerging as contrast agents for MRI. The safety of USPIO nanoparticles in humans has been established,[24] with degradation occurring through normal physiological iron (Fe)-handling pathways. Because of their smallness and good biocompatibility, USPIO nanoparticles can be linked to specific target molecules to achieve molecular tracing. Leung showed that sLe^X can be conjugated to USPIO nanoparticles and used to target E-selectin using MRI in a model of hepatitis.[25] We wished to develop a molecular probe to target E-selectin. Then, we wanted to apply it in vivo to evaluate the metastasis of NPC-xenografted tumors.

Methods

Ethical approval of study protocol

This study was undertaken in strict accordance with the recommendations in the *Guide for the Care and Use of Laboratory Animals* (National Institutes of Health [NIH], Bethesda, MD, USA). The study protocol was approved by the Ethics Committee of the Cancer Prevention and Research Institute of Guangxi Zhuang Autonomous Region (Nanning, China).

Materials

sLe^x was purchased from Carbosynth (Compton, UK). Oleic acid, $Fe(acac)_3$, oleylamine, *N*-hydroxysuccinimide (NHS), ethyl-3-(3-dimethylaminopropyl)carbodiimide (EDC), phenyl ether, 2-(*N*-morpholino)ethanesulfonic acid (MES), borax solution, and borate solution were purchased from Aladdin (Shanghai, China). Hexane, ethanol, and chloroform were obtained from Sinopharm Chemical Reagents (Shanghai, China). DSPE–polyethylene glycol ($PEG_{2,000}$) was purchased from AVT Pharmaceuticals (Shanghai, China). All chemical reagents were used without further purification.

Synthesis of USPIO

USPIO was synthesized by hydrothermal and high-temperature reactions assisted by autoclaves in accordance with the work of Sun et al.[26] USPIO nanoparticles were grown by high-temperature (200°C) decomposition of $Fe(aca)_3$ (2 mmol) in the presence of 1,2-hexadecanediol (10 mmol) and the surfactants oleic acid (6 mmol) and oleylamine (6 mmol) in phenyl ether (20 mL) for 1 hour and then heated to 265°C for 30 minutes. After cooling to room temperature, ethanol (40 mL) was added to the mixture under ambient conditions. We obtained black products via centrifugation (6,000 rpm for 10 minutes at room temperature). The black precipitate was dispersed in hexane–toluene. Centrifugation (6,000 rpm for 10 minutes at room temperature) was applied to remove undispersed residue. We repeated the process of ethanol precipitation and hexane–toluene dispersion twice or thrice, and Fe_3O_4 nanoparticles of diameter 6 nm were prepared. The Fe_3O_4 nanoparticles (84 mg) obtained were dispersed in hexane (4 mL). $Fe(acac)_3$ (2 mL), 1,2-hexadecanediol (10 mmol), phenyl ether (20 mL), oleic acid (6 mmol), and oleylamine (6 mmol) were added to the solvent. Following the procedures described in the synthesis of 6 nm nanoparticles, USPIO nanoparticles of diameter 10 nm coated with oleic acid as a surfactant were produced.

Synthesis of USPIO-PEG nanoparticles

We wished to functionalize Fe_3O_4 nanoparticles with PEG to increase the biocompatibility of Fe_3O_4 nanoparticles. Briefly, 50 mg DSPE-$PEG_{2,000}$ solid power dissolved in chloroform (5 mL) was added and mixed with 5 mL USPIO nanoparticles (Fe concentration of 1 mg/mL, dispersed in chloroform) at 70°C in a round-bottomed flask (50 mL) to permit sonication for 10 minutes. Then, 5 mL deionized water was added to and mixed with the samples in the round-bottomed flask. The latter was placed on a rotary evaporator, the vacuum turned on, and tlowered into a water bath at 70°C. The vacuum was released upon solvent evaporation. Fe_3O_4 nanoparticles with oleic acid as a surfactant coated with water-soluble DSPE-$PEG_{2,000}$

were prepared. The sample was passed through a 220 nm filter. Ultrafiltration was carried out to remove the lower precipitate and retain the upper black transparent solvent. The sample was labeled USPIO-PEG.

Synthesis of USPIO-PEG-sLe^x nanoparticles

First, buffer solutions were prepared. MES powder (213 mg) was dissolved in deionized water and made up to 50 mL. Then, the pH was adjusted to 5.5 so that an MES buffer was formed. Borax solution (3 mL, 0.05 mol/L) was mixed with 7 mL borate solution (0.2 mol/L) and diluted with deionized water to 100 mL. Then, the pH was adjusted to 8.3 so that a binding buffer (BB) was formed. USPIO-PEG (5 mL, Fe concentration of 1 mg/mL) was dispersed in 20 mL MES buffer. EDC powder (180 mg) and NHS powder (200 mg) were added to the MES buffer in turn. After adequate dissolution, the samples were agitated in a shaker at 150 rpm for 25 minutes to ensure sufficient activation of carboxyl (COOH) groups on the surface of the magnetic nanocrystals. At the end of activation, ultrafiltration, centrifugation, and washing (thrice) with deionized water were carried out to remove excess EDC and NHS. The sample was dispersed in 20 mL BB. Then, 2 mg sLe^X (distributed in BB) was added and the mixture allowed to incubate at room temperature in a shaker (150 rpm) for 2 hours. After ultrafiltration, centrifugation, and washing thrice with deionized water, the solution of UPSIO-PEG-sLe^X nanoparticles underwent dynamic light scattering (DLS) using a Zetasizer Nano ZSP (Malvern Instruments, Malvern, UK). The ζ-potential was obtained and the UPSIO-PEG-sLe^X nanoparticles stored at 4°C.

Characterization of nanoparticles

The shape, diameter, and distribution of UPSIO-PEG-sLe^X nanoparticles were measured by transmission electron microscopy (TEM) using a JEM-200CX system (JEOL, Tokyo, Japan) at 80 kV. UPSIO-PEG-sLe^X nanoparticles were diluted to 1 mg/mL with ultrapure water (pH 6). A small drop of UPSIO-PEG-sLe^X nanoparticles was placed in a wax plate and 2% phosphotungstic acid added dropwise to negatively stain the emulsion. Samples were air-dried on a copper grid. The diameter of 50 UPSIO-PEG-sLe^X nanoparticles was measured thrice, and the average value taken.

The hydrodynamic size and polydispersity index of USPIO-PEG nanoparticles and USPIO-PEG-sLe^X nanoparticles were measured by DLS using the Zetasizer Nano ZSP. The ζ-potential of USPIO-PEG nanoparticles and USPIO-PEG-sLe^X nanoparticles was measured by a 4700 Autosizer (Malvern Instruments). Component changes in nanoparticles of USPIO, USPIO-PEG, and USPIO-PEG-sLe^X were analyzed by thermogravimetric analysis (TGA). Fourier-transform infrared (FTIR) spectroscopy was carried out using a Nicolet 560 (Thermo Fisher Scientific, Waltham, MA, USA) at a resolution of 4 cm^{-1} in the range 4,000–400 cm^{-1}. Relaxation rates were measured on a MQ60 nuclear MR analyzer (Bruker, Billerica, MA, USA). USPIO-PEG-sLe^X nanoparticles were configured separately as a series of samples by stepwise dilution (0.2, 0.4, 0.6, 0.8, and 1.0 mM), and the test tubes were placed in a water bath at 37°C.

MRI in vivo

Twelve male and female BALB/C nude mice (aged 4–6 weeks) were obtained from the Laboratory Animal Center of Guangxi Medical University (license for production of laboratory animals, SCXK 2014–0002; license for use of laboratory animals, SYXK 2014–0003). Mice were maintained under specific pathogen-free conditions. For creation of a model of metastasis to inguinal lymph nodes, 2×10^6 per 20 μL saline of 5-8F cells were injected into the left footpads of mice. MRI was undertaken after 8 weeks of growth.

MRI was conducted using a 3 T MRI scanner (Discovery MR750; GE Healthcare, Little Chalfont, UK) with a dedicated four-channel coil (10F-04885; Teshen, Shenzhen, China) with mice in the prone position. Anesthesia was maintained with 0.1 mL lidocaine (Ousuka, Tianjin, China). Four scans were carried out for each mouse. The first scan (t0) was done before administration of USPIO-PEG-sLe^X nanoparticles (0.1 mL) via the tail vein. The other scans were carried out at 0 (t1), 1 (t2), and 2 hours (t3) postinjection. Coronal T2-weighted images were obtained to observe the xenografted tumor and metastasis. Then, axial T1-weighted images (repetition time [TR] and echo time [TE] of 663 ms and 20 ms, respectively) and T2-weighted images (TR 2,000 ms and TE 60 ms) were obtained. Subsequently, T2* was undertaken at the same location using a multishot, multislice, fast-field echo sequence of 300 ms/2.5–22.3 ms TR/TE with eight echo times and a 2.8 ms interval between two echoes, 2 mm slice thickness, 256×256 matrix size, 80 mm field of view, and 30° flip angle.

T2* color-coded pixel mapping was reconstructed using Functool modules (GE Global Research, New York, NY, USA). For quantitative analyses, regions of interest (ROIs) were drawn manually by two fellowship-trained readers. The ROIs chosen were those outside the tumor to permit normalization of three maximum sections

through the tumor on T2* mapping. Mean T2* relaxation times (T2* value) at the four time points (t0–t3) were calculated. Changes in T2* (ΔT2*) and enhancement rate (ER) at t1, t2, and t3 were calculated based on the T2* value at t0:

$$\Delta T2^{*} = Mo - Mt$$

$$ER = (Mo - Mt)/Mo \times 100\%$$

where Mo is the T2* value at t0 and Mt is the T2* value at t1, t2, or t3.

Tumor staining and E-selectin immunohistochemistry

After MRI, all mice were killed. Their footpad tumors and metastatic lymph nodes were removed and fixed with 10% formaldehyde solution. Next, 4 μm paraffin slices were prepared for routine H&E staining. Morphology was observed by light microscopy and immunohistochemical (IHC) analyses. Mice were divided into a metastasis group and control (metastasis-free) group according to H&E staining.

For IHC analyses, immunostaining with anti-CD62E (mouse monoclonal antibody; Merck, Whitehouse Station, NJ, USA) was done. Sections were stained with a streptavidin–peroxidase kit (catalog number 9720; Maixin, Shenzhen, China). The chromogen used was 3,3′-diaminobenzidine (Maixin), which was slightly counterstained with hematoxylin, dehydrated, and mounted. To ascertain if metastasis promoted E-selectin expression in vivo, images were processed using ImageJ (NIH). The mean optical density (MOD) provided an indirect assessment of E-selectin expression. All images were evaluated by two observers blinded to experimental groupings.

Statistical analyses

Data are expressed as mean ± SD. Image parameters collected were the T2* value, ΔT2* value, and ER at four times. The IHC parameter collected was the MOD. Univariate analysis was undertaken using ANOVA to compare image parameters and MOD between the metastasis group and control group. To evaluate the association between image parameters, metastasis, and time, we undertook two-way repeated-measures ANOVA. Spearman's correlation coefficient was used to assess the association between image parameters and MOD. All statistical computations were carried out with SPSS 18.0 (IBM, Armonk, NY, USA). $P<0.05$ was considered significant.

Results

Characterization of USPIO-PEG-sLe^{x} nanoparticles

The USPIO-PEG-sLe^{X} nanoparticles obtained were black without obvious precipitates, and were able to be dispersed readily in nonpolar solvents. Figure 1 shows TEM images of USPIO-PEG-sLe^{X} nanoparticles negatively stained with 2% phosphotungstic acid. These USPIO-PEG-sLe^{X} nanoparticles were nearly spherical. USPIO-PEG-sLe^{X} nanoparticles were distributed uniformly and had a size of 10±2.6 nm. DLS indicated that the average size of USPIO-PEG nanoparticles and USPIO-PEG-sLe^{X} nanoparticles was 34.06±9.95 nm and 53.35±16.99 nm and that the polydispersity index was 0.186 and 0.499, respectively (Figure 2). The distribution of nanoparticle size was narrow.

The ζ-potential of USPIO-PEG nanoparticles and USPIO-PEG-sLe^{X} nanoparticles was 11.6±3.96 mV and −12.6±5.33 mV, respectively (Figure 3). The ζ-potential of USPIO-PEG nanoparticles was positive due to their terminal amino-acid groups. After conjugation with sLe^{X}, the ζ-potential became negative, because sLe^{X} bonded to the terminal amino-acid groups of the nanoparticles by its COOH groups and because the phosphate groups on the PEG surface were negative.

According to data for hydrodynamic size and changes in the ζ-potential, coupling of the USPIO-PEG-sLe^{X} group was deemed to be successful. The TGA profiles of nanoparticles of USPIO, USPIO-PEG, and USPIO-PEG-sLe^{X} are shown in Figure 4. At 100°C–750°C, the weight loss of nanoparticles of USPIO, USPIO-PEG, and USPIO-PEG-sLe^{X} was 48.27%, 55.73%, and 66.94%, respectively.

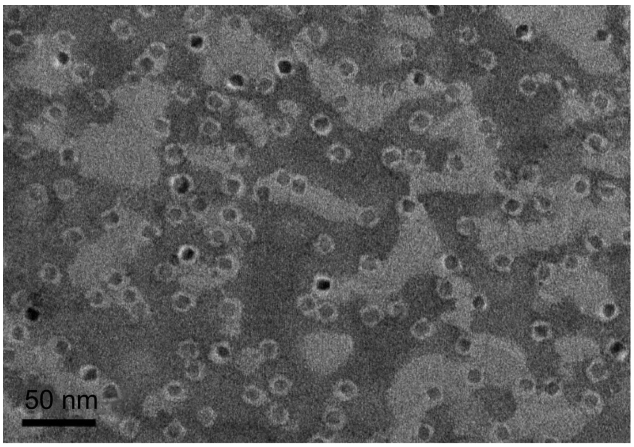

Figure 1 Negatively stained transmission electron microscopy (TEM) of the ultrasmallsuperparamagnetic iron oxide (USPIO)–polyethylene glycol (PEG)–Sialyl Lewis X (sLe^{x}) nanoparticles. The nanoparticles are well separated by the PEG shell.

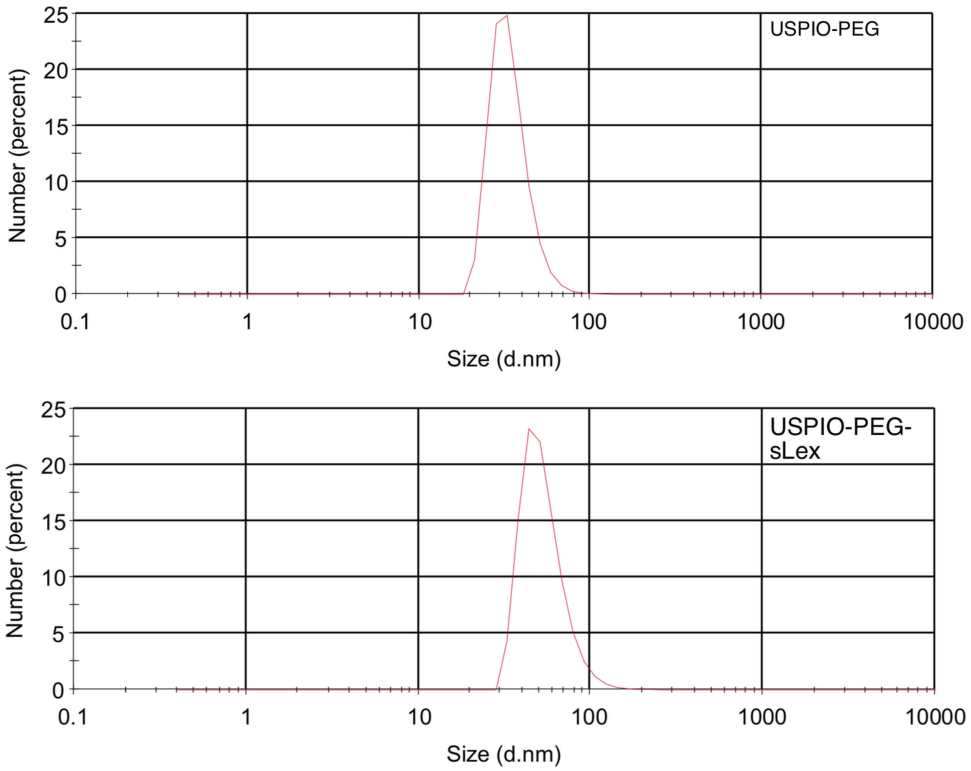

Figure 2 Dynamic light scattering (DLS) of ultrasmall superparamagnetic iron oxide (USPIO)–polyethylene glycol (PEG) and USPIO-PEG–Sialyl Lewis X (sLe^x).

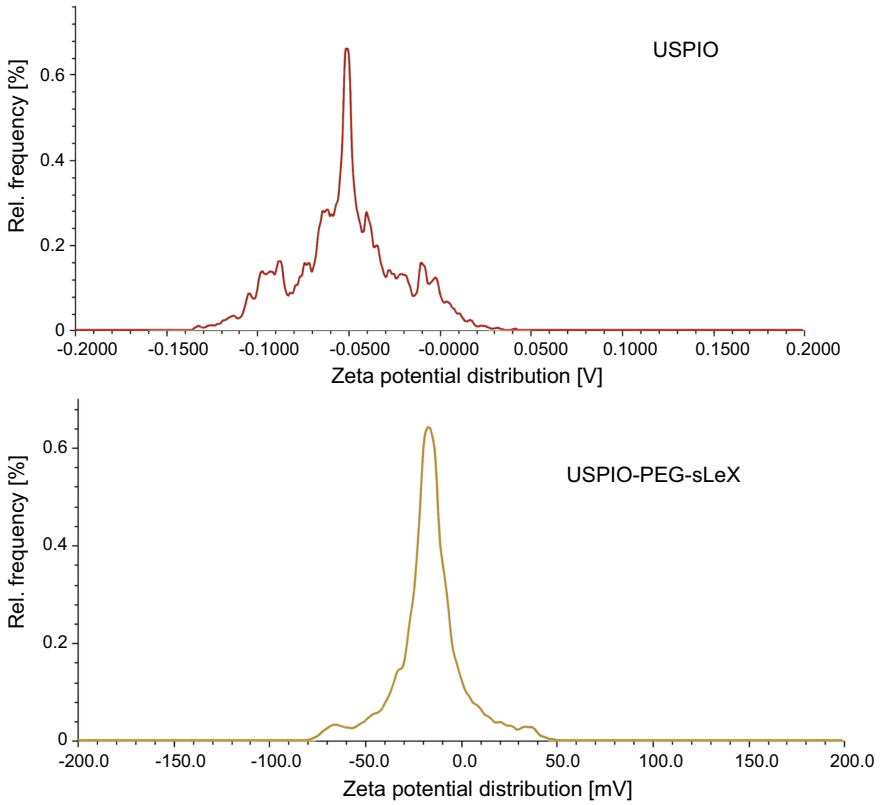

Figure 3 ζ-potential of ultrasmall superparamagnetic iron oxide (USPIO)–polyethylene glycol (PEG) and USPIO-PEG–Sialyl Lewis X (sLe^x).

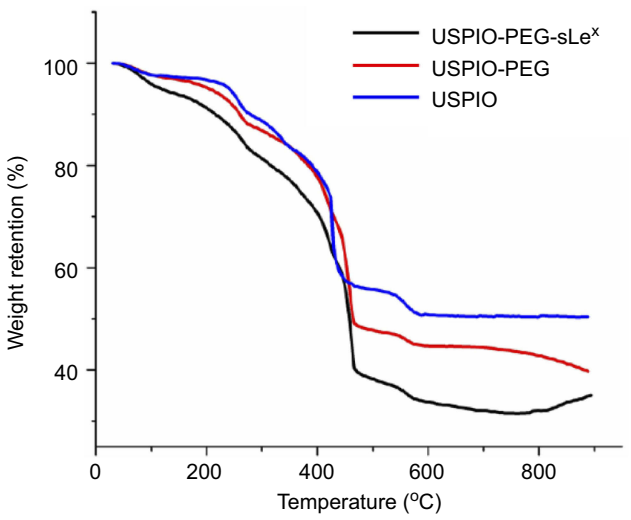

Figure 4 Thermogravimetric analysis (TGA) of ultrasmall superparamagnetic iron oxide (USPIO), USPIO–polyethylene glycol (PEG), and USPIO-PEG–Sialyl Lewis X (sLe^x).

FTIR spectra are shown in Figure 5. The absorption peak of the carbonyl (C=O) stretching vibration (1,723.7 cm^{-1}) was decreased. Peaks at 1,632.4 cm^{-1} and 1,567.1 cm^{-1} appeared, which were the asymmetric and symmetric absorption peaks of –COO– groups, respectively, which suggested that the surface of USPIO contained many COOH groups. Peaks at 1,059.5 cm^{-1} and 1,126.5 cm^{-1} appeared in FTIR spectra after PEG coupling, which were due to a C–OH stretching vibration and C–O–C stretching vibration of PEG. The FTIR spectra and TGA results confirmed that sLe^x was immobilized on nanoparticles.

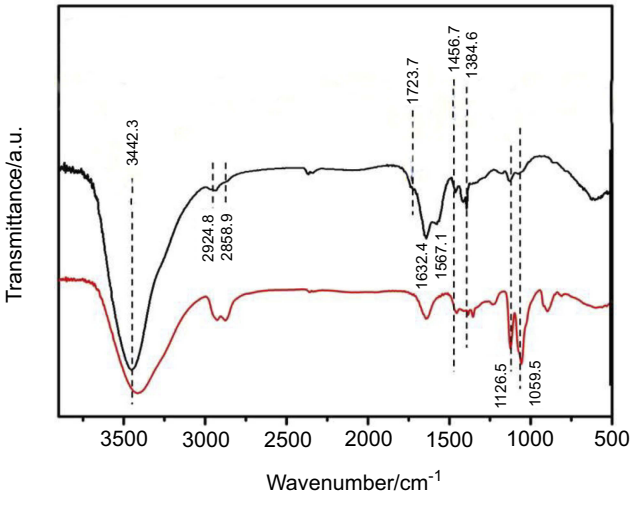

Figure 5 Fourier-transform infrared (FTIR) spectra of ultrasmall superparamagnetic iron oxide (USPIO; (black) and USPIO–polyethylene glycol (PEG)–Sialyl Lewis X (sLe^X; red).

MRI relaxivity of USPIO-PEG-sLe^x nanoparticles

MR relaxivity (r1=1/T1; r2=1/T2) of USPIO-PEG-sLe^X nanoparticles suspended in deionized water was measured at different Fe concentrations. USPIO-PEG-sLe^X nanoparticle r1 and r2 were linearly proportional to the Fe concentration (Figure 6): r1 and r2 weres 9.8 and 28.8 mM/s, respectively (Figure 6).

Uptake of USPIO nanoparticles in vivo

Mice were excluded if they had not undergone four complete MRI scans. As such, the data of eleven mice were included in this analysis. H&E staining revealed that six of the eleven (54%) were classified as the metastasis group and five (45%) as the control (nonmetastasis) group. A primary tumor in a footpad and a tumor in an inguinal lymph node in the metastasis group are shown in Figure 7. Image parameters (T2* value, ΔT2* value, ER) of the footpad tumors in the two groups before and after injection of USPIO-PEG-sLe^X nanoparticles are given in Table 1.

No significant difference was found with regard to T2* values before injection of USPIO-PEG-sLe^X nanoparticles (t0) between the metastasis group and control group (P=0.390, Figure 8). At 0 (t1), 1 (t2), and 2 hours (t3) after administration of USPIO-PEG-sLe^X nanoparticles, T2* values of tumors in the metastasis group were significantly lower than the control group (P=0.005, 0.008, and 0.019, respectively). ΔT2* values

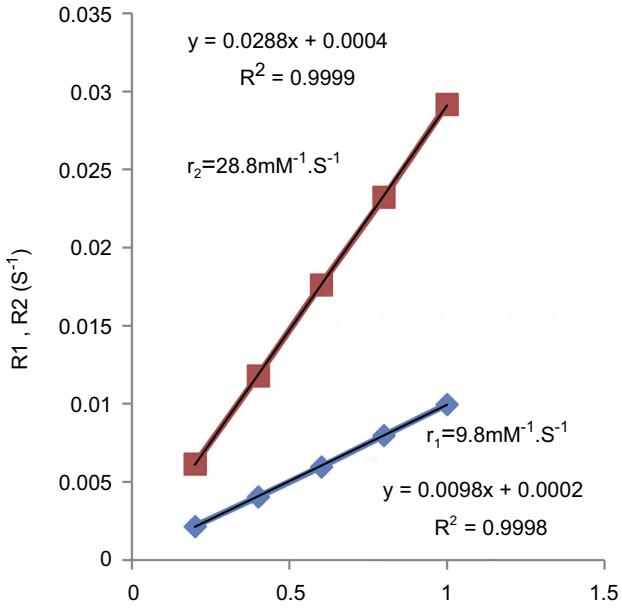

Figure 6 Relaxivity (R1 and R2) versus ultrasmall superparamagnetic iron oxide (USPIO)–polyethylene glycol (PEG)–Sialyl Lewis X (sLe^X) concentration.

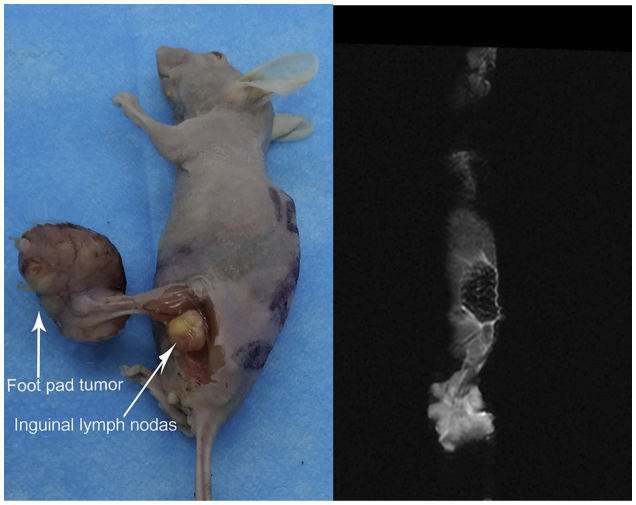

Figure 7 Representative images of primary footpad tumor and metastatic inguinal lymph nodes.

of tumor at t1, t2, and t3 in the metastasis group were significantly higher than the control group (P=0.027, 0.048, and 0.043, respectively). There was a significant difference in ER at t1, t2, and t3 between the metastasis group and control group (P=0.001, 0.005, and 0.007, respectively, Figure 8). Figure 9 shows the axial T2* mapping images resulting from injection of USPIO-PEG-sLe^X nanoparticles in mice of the metastasis group and control group.

Two-way repeated-measures ANOVA was used to assess changes in T2* value over time, as well as differences between the metastasis group and control group (Figure 10). There was a significant interaction between groups and time for T2* value after administration of USPIO-PEG-sLe^X nanoparticles (P=0.029). A significant difference was observed for the within-group change from t0 to t3 (P=0). T2* values started to decrease after administration of USPIO-PEG-sLe^X nanoparticles, and decreased obviously at t1 and t2 in both groups. The T2* value of the metastasis group increased slightly at t3, whereas that in the control group continued to decrease. Maximum enhancement of the slope at t1 was significantly higher in the metastasis group than the control group. These changes in T2* value were clearly visible upon T2* mapping (Figure 9).

MRI of E-selectin expression

IHC analyses were employed to assess E-selectin expression in tumor sections under high-power fields (400×, Figure 11). E-selectin was expressed in all tumor tissues. E-selectin staining was mainly in the membranes of tumor cells. The MOD of the metastasis group and control group was 0.525±0.243 and 0.082±0.012, respectively, and this difference was significant (P=0.007, Figure 12). Therefore, E-selectin expression had increased significantly in the metastasis group.

Table 1 Image parameters and mean optical density (MOD) of primary tumors in footpads in the metastasis group and control group

Parameter	Metastasis group (n=6)	Control group (n=5)	*F*	*P*
T2* value, t0 (ms)	22.25±8.08 (13.78 to 30.73)	27.01±9.45 (15.27 to 38.76)	0.814	0.390
T2* value, t1 (ms)	11.57±4.02 (7.35 to 15.78)	24.82±7.84 (15.07 to 34.56)	13.169	0.005
T2* value, t2 (ms)	10.09±4.88 (4.97 to 15.21)	24.15±8.74 (13.30 to 35.00)	11.435	0.008
T2* value, t3 (ms)	12.46±5.63 (6.55 to 18.37)	23.42±7.12 (14.57 to 32.26)	8.149	0.019
ΔT2* value, t1 (ms)	10.69±6.23 (4.15 to 17.23)	3.86±2.20 (−2.60 to 7.00)	6.966	0.027
ΔT2* value, t2 (ms)	12.17±8.67 (3.06 to 21.27)	2.87±1.37 (−0.50 to 6.24)	5.224	0.048
ΔT2* value, t3 (ms)	9.80±3.03 (5.56 to 14.03)	4.32±2.28 (−2.22 to 9.42)	5.563	0.043
Enhancement rate (ER), t1 (%)	45.98±14.03	7.10±5.18	22.393	0.001
ER, t2 (%)	51.15±22.70	11.04±6.01	13.288	0.005
ER, t3 (%)	44.05±13.92	12.09±7.54	12.361	0.007
MOD	0.53±0.24 (0.27 to 0.78)	0.082±0.012 (0.07 to 0.10)	19.850	0.007

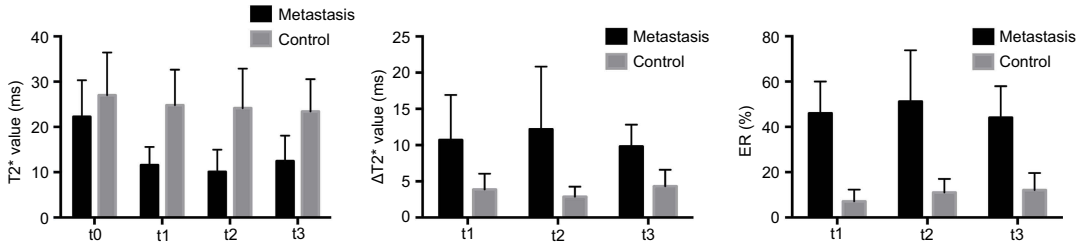

Figure 8 T2* value, ΔT2* value and enhancement rate (ER) at different time points in metastasis group and control group.

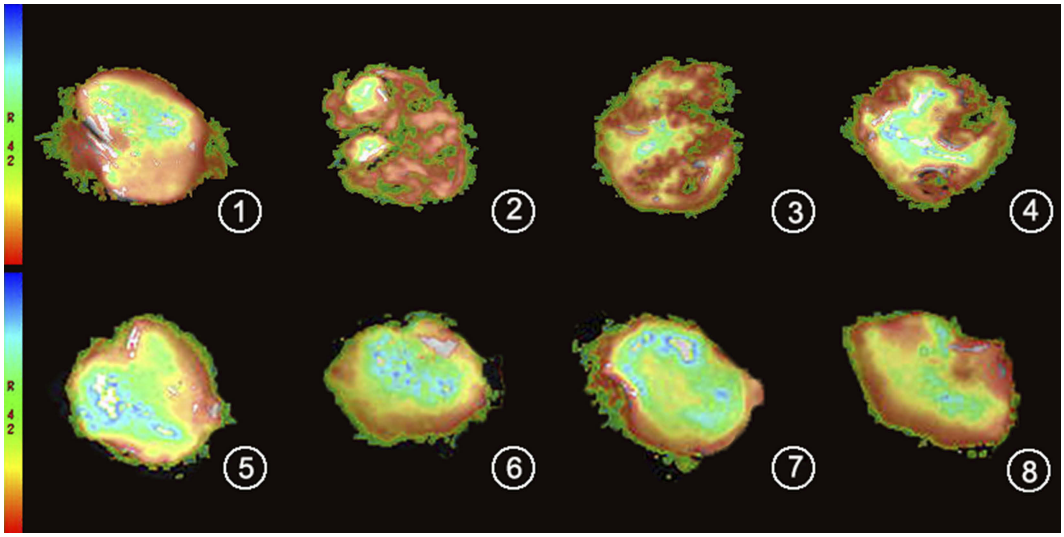

Figure 9 T2* mapping shows effect of ultrasmall superparamagnetic iron oxide (USPIO)–polyethylene glycol (PEG)–Sialyl Lewis X (sLe^X) contrast agent on images of primary tumors in footpads.
Notes: Color scale used for magnetic resonance imaging (MRI) signal-intensity mapping with software. Top row, T2* mapping of metastasis group at t0, t1, t2, and t3. Bottom row, T2* mapping of control group at t0, t1, t2, and t3. In both mice, USPIO-PEG-sLex was administered via the tail vein.

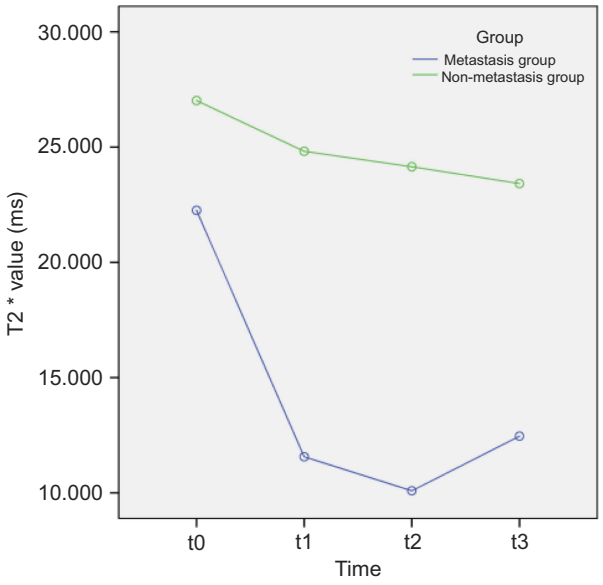

Figure 10 T2* of primary tumors in footpads in metastasis group and control group before and after intravenous administration of ultrasmall superparamagnetic iron oxide (USPIO)–polyethylene glycol (PEG)–Sialyl Lewis X (sLe^X).
Notes: There was a rapid decrease in mice with metastasis that were given the targeting agent USPIO-PEG-sLe^X. T2* changes in tumors in the control group were relatively gentle. Data points are show mean ± SD.

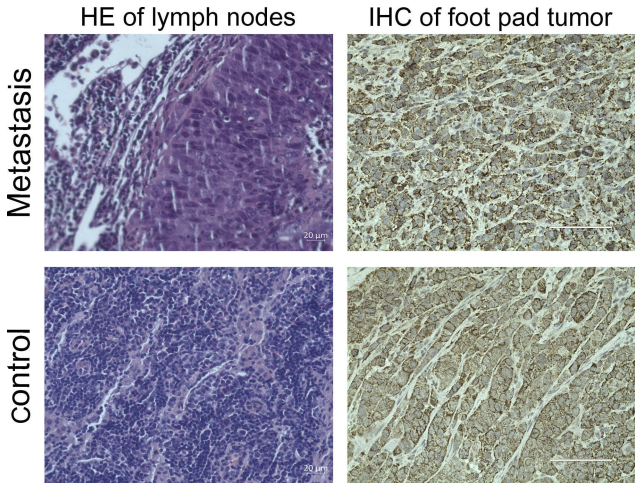

Figure 11 Results of histological examination of lymph (H&E stain, original magnification 400×) and transplanted tumors (immunohistochemical [IHC], original magnification 400×).
Notes: Top row, metastasis group; bottom row, control group.

Associations between image parameters and MOD were calculated by Spearman's correlation coefficient (Table 2). Six parameters (T2* at t2, ΔT2* at t1, ΔT2* at t2, ER at t1, ER at t2, and ER at t3) were related to MOD, and Spearman's correlation coefficients were −7.00, 0.655, 0.682, 0.718, 0.755, and 0.636(P=0.016, 0.029, 0.021, 0.013, 0.007, and 0.035, respectively). The maximum correlation coefficient for ER was at t2 (Figure 13).

Discussion

Imaging probes require ligands that can bind to cell biomarkers with high sensitivity, specificity, and affinity.[27] In our study, sLe^X was a conjugating agent and USPIO provided a signal that could be measured. E-selectin has a major role during the multistep process of metastasis.[28,29] Kaila et al reported on the synthesis of sLe^X analogues that can bind to E-selectin.[30]

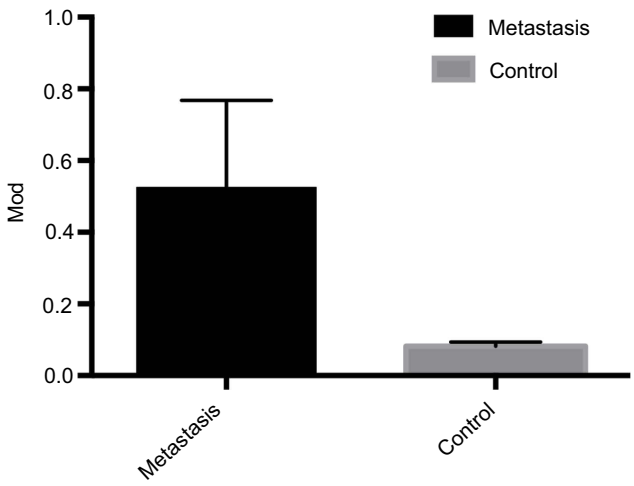

Figure 12 Immunohistochemical (IHC) staining in metastasis group and control group. E-selectin preferentially upregulated in metastasis group.
Abbreviation: MOD, mean optical density.

Table 2 Associations between image parameters and mean optical density assessed by Spearman's correlation coefficient

Parameter	Correlation coefficient	*P*
T2* value, t1	−0.573	0.066
T2* value, t2	−7.00	0.016
T2* value, t3	−4.445	0.170
ΔT2* value, t1	0.655	0.029
ΔT2* value, t2	0.682	0.021
ΔT2* value, t3	0.564	0.071
Enhancement rate (ER), t1	0.718	0.013
ER, t2	0.755	0.007
ER, t3	0.636	0.035

USPIO has been explored extensively for cell labeling, MRI contrast agents, and drug delivery.[31–35] USPIO has been shown to change the relaxation rate of water protons detected by MRI. MRI relaxometry using multiple echo times is the imaging reference standard for Fe quantification, because the R2/R2*/T2* value has been shown to be directly proportional to the Fe concentration in tissue.[36–38] As such, T2* mapping can be used to reveal the distribution of the USPIO-PEG-sLe^X nanoparticles, which in turn reflects the distribution of E-selectin expression. PEG was used to increase the hydrophilicity of nanoparticles. Studies have shown that PEG on nanoparticles is important for higher stability, longer cycle times, and biocompatibility.[39,40]

In the present study, FTIR spectroscopy, TEM, DLS, TGA, and MRI relaxation tests revealed the composition and magnetic properties of synthesized nanoparticles. FTIR spectroscopy showed that sLe^X was coated on the surface of USPIO. TEM images revealed that USPIO-PEG-sLe^X nanoparticles were well dispersed. DLS demonstrated that hydrodynamic dimensions were increased and that the distribution of nanoparticle size was narrow. Control of the size of monodispersed nanoparticles is very important, because the properties of nanocrystals are strongly dependent upon the dimension of nanoparticles.[41] The increase in the ζ-potential suggested that our molecular probe had high stability.[42] TGA revealed that nanoparticles of USPIO, USPIO-PEG, and USPIO-PEG-sLe^X had a gradient of thermal weight loss and that USPIO-PEG-sLe^X nanoparticles had a lower initial decomposition temperature and the fastest weight loss. TGA also confirmed that sLe^X was coated on USPIO-PEG. Figure 6 demonstrates that USPIO-PEG-sLe^X nanoparticles exhibited negative contrast enhancement. Therefore, USPIO-PEG-sLe^X nanoparticles were prepared and evaluated as targeted MRI contrast agents.

In vivo results showed that T2* values in the metastasis group was significantly lower the control group after administration of USPIO-PEG-sLe^X nanoparticles. The ΔT2* value and ER were higher in the metastasis group than the control group. Considering that E-selectin had increased in the metastatic group, more affinity components sLe^X target the molecular probe to the footpad xenograft tumor. USPIO can shorten T1 and T2/T2* relaxation processes, but is used mainly as a T2 contrast agent in MRI. The T2* value decreases with an increase in USPIO concentration.[43,44] These results suggest that E-selectin can bind to molecular probes with high specificity and that it could be a feasible target to identify NPC metastasis. USPIO-PEG-sLe^X nanoparticles could be "ideal" MRI molecular probes because of their high selectivity and affinity for the target biomolecule (E-selectin).

We found interactions between groups and time for the T2* value after administration of USPIO-PEG-sLe^X nanoparticles. T2* values decreased obviously at t1 and t2 in both groups. Changes in T2* values in the two groups were different. Maximum enhancement of the slope at t1 was significantly higher in the metastasis group than the control group, and this could have been due to two main factors. First, the number of E-selectin molecules in the two groups of tumor tissues was different, so the concentration and distribution of molecular probes in the tissues were different. The significant decrease in T2* values in the metastatic group suggested that the molecular probes had a significant signal-amplification effect. Second, studies have shown that invasive tumors are characterized by increased volume and permeability in blood vessels.[45] High permeability was important in our study to ensure that USPIO-PEG-sLe^X nanoparticles reached the target

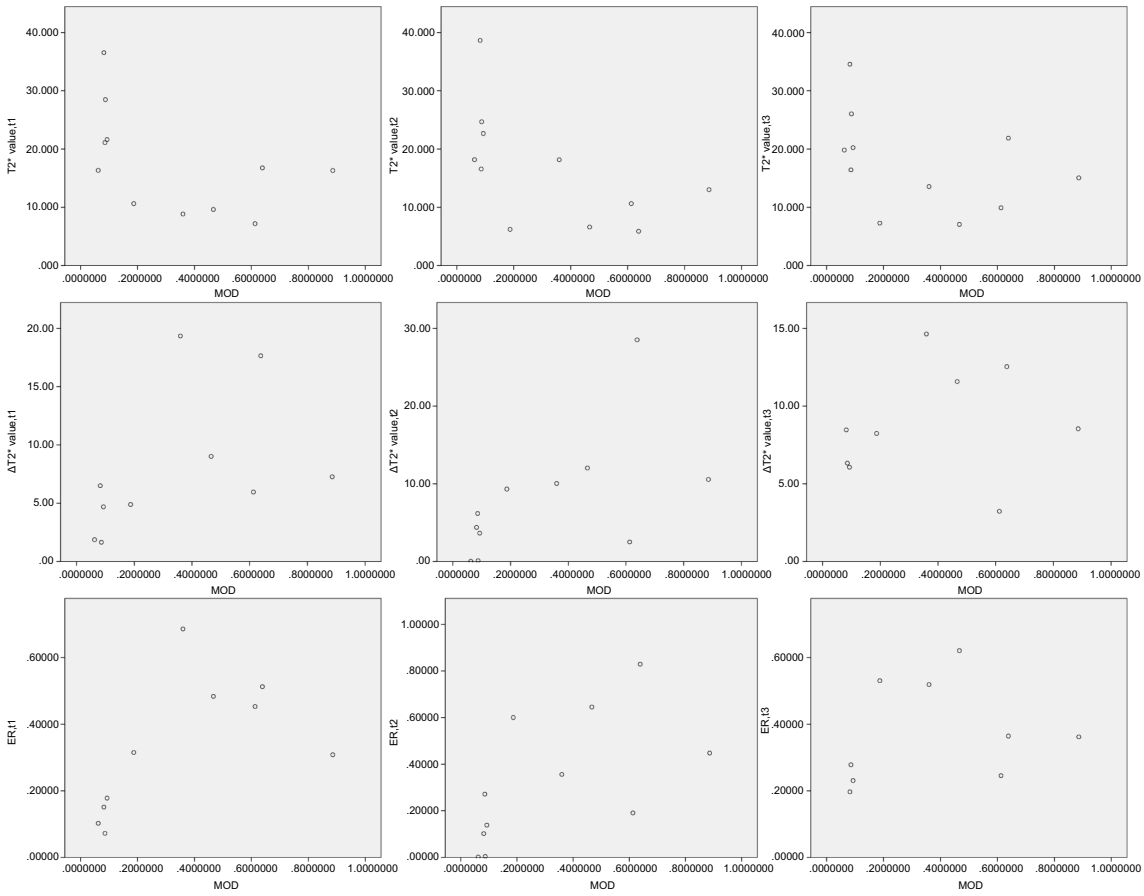

Figure 13 Correlations among image parameters.
Notes: T2* value, ΔT2* value, and enhancement rate (ER) of t1, t2, and t3 and mean optical density (MOD; calculated from immunohistochemistry images by ImageJ). Six parameters (T2* value [t2], ΔT2* value [t1,t2], and ER [t1, t2, and t3]) were related to the MOD. Neither T2* value (t1 and t3) nor ΔT2* value (t3) correlated with MOD.
Abbreviation: MOD, mean optical density.

rapidly. Our results are in accordance with those of studies showing that sLe^X mimetics allow USPIO in molecular probes to interact with E-selectin.[25,46,47]

In the metastasis group, maximum enhancement of the slope was at t1, whereas the maximum ER was at t2. These data are in accordance with results from Boutry et al, who demonstrated that relative signal enhancement (negative) was significantly higher 1 hour after injection of USPIO-g-sLe^X nanoparticles.[48] T2* values in the control group showed a continuous, slow decline. Our observation of changes in T2* in the metastasis group could be due to two main factors. First, USPIO has a long half-life in plasma: ~24 hours in humans[49] and 2 hours in mice.[50] Second, E-selectin expression in the metastasis group tended to be saturated at t2, and then T2* values increased slightly. Therefore, sLe^X labeling targeted E-selectin with high contrast quickly.

MOD was used to measure E-selectin expression in xenograft tumors. MOD in the metastasis group was significantly higher than the control group. Such high expression of E-selectin in the metastasis group suggests that E-selectin expression in NPC promotes NPC metastasis. The ER at each time point was related to the MOD. The ER revealed the distribution of USPIO-PEG-sLe^X nanoparticles, which in turn reflected the distribution of E-selectin expression. Therefore, the ER aided determination of the distribution of E-selectin expression in tumor tissue.

Our study had four main limitations. First, due to repeat MRI, the position of mice was changed over the four scans, so the ROI could not be matched completely. Second, ROI analyses were done on T2* mapping by selecting only the three sections showing the maximum diameter of the tumor, which may not have been representative of the entire tumor. Third, associations between MOD and image parameters were obtained from only eleven mice. Fourth, our results of MRI parameters might not apply to those of other institutions, particularly those that use different MRI methods.

Conclusion

We showed that E-selectin expression in vivo during metastasis can be depicted with as-prepared USPIO-PEG-sLe^X nanoparticles by MRI. Use of such molecular probes could enable detection of early metastasis of NPC, more accurate staging, and treatment monitoring.

Acknowledgments

This work was supported financially by the National Natural Science Foundation of China (81260334, 81760533, 81460452).

Disclosure

The authors report no conflicts of interest in this work.

References

1. Chua MLK, Wee JTS, Hui EP, Chan ATC. Nasopharyngeal carcinoma. *Lancet*. 2016;387(10022):1012–1024. doi:10.1016/S0140-6736(15)00055-0
2. Chan AT, Grégoire V, Lefebvre JL, et al. Nasopharyngeal cancer: EHNS-ESMO-ESTRO clinical practice guidelines for diagnosis, treatment and follow-up. *Ann Oncol*. 2012;23(Suppl 7):83–85. doi:10.1093/annonc/mds266
3. Saba NF, Salama JK, Beitler JJ, et al. ACR Appropriateness criteria® for nasopharyngeal carcinoma. *Head Neck*. 2016;38(7):979–986. doi:10.1002/hed.24423
4. Wei WI, Sham JS. Nasopharyngeal carcinoma. *Lancet*. 2005;365(9476):2041–2054. doi:10.1016/S0140-6736(05)66698-6
5. Hui E, Leung S, Au J, et al. Lung metastasis alone in nasopharyngeal carcinoma: a relatively favorable prognostic group. A study by the Hong Kong nasopharyngeal carcinoma study group. *Cancer*. 2004;101(2):300–306. doi:10.1002/cncr.20358
6. Gout S, Tremblay PL, Huot J. Selectins and selectin ligands in extravasation of cancer cells and organ selectivity of metastasis. *Clin Exp Metastas*. 2008;25(4):335–344. doi:10.1007/s10585-007-9096-4
7. Yasmin-Karim S, King MR, Messing EM, Lee YF. E-selectin ligand-1 controls circulating prostate cancer cell rolling/adhesion and metastasis. *Oncotarget*. 2014;5(23):12097–12110. doi:10.18632/oncotarget.2503
8. Carrascal M, Silva M, Ferreira J, et al. A functional glycoproteomics approach identifies CD13 as a novel E-selectin ligand in breast cancer. *Biochim Biophys Acta*. 2018;1862(9):2069–2080. doi:10.1016/j.bbagen.2018.05.013
9. Xia HZ, Du WD, Qiang W, et al. E-selectin rs5361 and FCGR2A rs1801274 variants were associated with increased risk of gastric cancer in a Chinese population. *Mol Carcinogen*. 2012;51(8):597–607. doi:10.1002/mc.20828
10. Aychek T, Miller K, Sagi-Assif O, et al. E-selectin regulates gene expression in metastatic colorectal carcinoma cells and enhances HMGB1 release. *Int J Cancer*. 2008;123(8):1741–1750. doi:10.1002/ijc.23375
11. Zhang B, Chen H, Yao X, Cong W, Wu M. E-selectin and its ligand-sLeX in the metastasis of hepatocellular carcinoma. *Hepatobiliary Pancreat Dis Int*. 2002;1(1):80–82.
12. Påhlsson P, Strindhall J, Srinivas U, Lundblad A. Role of N-linked glycosylation in expression of E-selectin on human endothelial cells. *Eur J Immunol*. 1995;25(9):2452–2459. doi:10.1002/(ISSN)1521-4141
13. Jubeli E, Moine L, Vergnaud-Gauduchon J, Barratt G. E-selectin as a target for drug delivery and molecular imaging. *J Control Release*. 2012;158(2):194–206. doi:10.1016/j.jconrel.2011.09.084
14. Bevilacqua M, Stengelin S, Gimbrone M, Seed B. Endothelial leukocyte adhesion molecule 1: an inducible receptor for neutrophils related to complement regulatory proteins and lectins. *Science*. 1989;243(4895):1160–1165.
15. Polley M, Phillips M, Wayner E, et al. CD62 and endothelial cell-leukocyte adhesion molecule 1 (ELAM-1) recognize the same carbohydrate ligand, sialyl-Lewis x. *Proc Natl Acad Sci USA*. 1991;88(14):6224–6228. doi:10.1073/pnas.88.14.6224
16. Silva M, Fung R, Donnelly C, Videira P, Sackstein R. Cell-specific variation in E-selectin ligand expression among human peripheral blood mononuclear cells: implications for immunosurveillance and pathobiology. *J Immunol*. 2017;198(9):3576–3587. doi:10.4049/jimmunol.1601636
17. Kang S, Blache C, Bajana S, et al. The effect of soluble E-selectin on tumor progression and metastasis. *BMC Cancer*. 2016;16:331. doi:10.1186/s12885-016-2366-2
18. Häuselmann I, Roblek M, Protsyuk D, et al. Monocyte induction of E-selectin-mediated endothelial activation releases VE-cadherin junctions to promote tumor cell extravasation in the metastasis cascade. *Cancer Res*. 2016;76(18):5302–5312. doi:10.1158/0008-5472.CAN-16-0584
19. Renkonen J, Paavonen T, Renkonen R. Endothelial and epithelial expression of sialyl Lewisx and sialyl Lewisa in lesions of breast carcinoma. *Int J Cancer*. 1997;74(3):296–300. doi:10.1002/(ISSN)1097-0215
20. Jin G, Liu S, Kang W, et al. Quantitative expression analysis of metastasis-related ELAM-1 in nasopharyngeal carcinoma. *Int J Clin Exp Med*. 2017;10(1):808–813.
21. Weissleder R, Mahmood U. Molecular imaging. *Radiology*. 2001;219(2):316–333. doi:10.1148/radiology.219.2.r01ma19316
22. Weissleder R, Cheng HC, Bogdanova A, Bogdanov A. Magnetically labeled cells can be detected by MR imaging. *J Magn Reson Imaging*. 2010;7(1):258–263. doi:10.1002/jmri.1880070140
23. Runge V. Current technological advances in magnetic resonance with critical impact for clinical diagnosis and therapy. *Invest Radiol*. 2013;48(12):869–877. doi:10.1097/01.rli.00004-34380.71793.d3
24. Taylor A, Panting J, Keegan J, et al. Safety and preliminary findings with the intravascular contrast agent NC100150 injection for MR coronary angiography. *J Magn Reson Imaging*. 1999;9(2):220–227. doi:10.1002/(SICI)1522-2586(199902)9:2<220::AID-JMRI11>3.0.CO;2-A
25. Leung K. *Molecular Imaging and Contrast Agent Database*. Bethesda, MD: National Center for Biotechnology Information; 2004.
26. Sun S, Zeng H, Robinson D, et al. Monodisperse MFe_2O_4 (M=Fe, Co, Mn) nanoparticles. *J Am Chem Soc*. 2004;126(1):273–279. doi:10.1021/ja047044i
27. Wang A, Farokhzad O. Current progress of aptamer-based molecular imaging. *J Nucl Med*. 2014;55(3):353–356. doi:10.2967/jnumed.113.126144
28. Zhong L, Huot J, Simard M. p38 activation induces production of miR-146a and miR-31 to repress E-selectin expression and inhibit transendothelial migration of colon cancer cells. *Sci Rep-UK*. 2018;8(1):2334. doi:10.1038/s41598-018-20837-9
29. Liu J, Liu Z, Hu X, Zhang Y, Zhang S. Synthetic E-selectin prevents postoperative vascular restenosis by inhibiting nuclear factor κB in rats. *Mol Med Rep*. 2018;17(4):5065–5073. doi:10.3892/mmr.2018.8572
30. Kaila N, Thomas B. Design and synthesis of sialyl Lewis(x) mimics as E- and P-selectin inhibitors. *Med Res Rev*. 2002;22(6):566–601. doi:10.1002/med.10018

31. Ma X, Tao H, Yang K, et al. A functionalized graphene oxide-iron oxide nanocomposite for magnetically targeted drug delivery, photothermal therapy, and magnetic resonance imaging. *Nano Res*. 2012;5(3):199–212. doi:10.1007/s12274-012-0200-y
32. Kazmierczak P, Schneider M, Habereder T, et al. αvß3-Integrin-targeted magnetic resonance imaging for the assessment of early antiangiogenic therapy effects in orthotopic breast cancer xenografts. *Invest Radiol*. 2016;51(11):746–755. doi:10.1097/RLI.0000000000000278
33. Jayapaul J, Arns S, Bunker M, et al. Evaluation of riboflavin receptor targeted fluorescent USPIO in mice with prostate cancer xenografts. *Nano Res*. 2016;9(5):1319–1333. doi:10.1007/s12274-016-1028-7
34. Patil US, Adireddy S, Jaiswal A, Mandava S, Lee BR, Chrisey DB. *In vitro/in vivo* toxicity evaluation and quantification of iron oxide nanoparticles. *Int J Mol Sci*. 2015;16(10):24417–24450. doi:10.3390/ijms161024417
35. Klohs J, Deistung A, Ielacqua G, et al. Quantitative assessment of microvasculopathy in arcAβ mice with USPIO-enhanced gradient echo MRI. *J Cereb Blood Flow Metab*. 2016;36(9):1614–1624. doi:10.1177/0271678X15621500
36. Kuhlpeter R, Dahnke H, Matuszewski L, et al. R2 and R2* mapping for sensing cell-bound superparamagnetic nanoparticles: in vitro and murine in vivo testing. *Radiology*. 2007;245(2):449–457. doi:10.1148/radiol.2451061345
37. Anderson LJ, Holden S, Davis B, et al. Cardiovascular T2-star (T2*) magnetic resonance for the early diagnosis of myocardial iron overload. *Eur Heart J*. 2001;22(23):2171–2179. doi:10.1053/euhj.2001.2822
38. Chavhan GB, Babyn PS, Thomas B, Shroff MM, Haacke EM. Principles, techniques, and applications of T2*-based MR imaging and its special applications. *Radiographics*. 2009;29(5):1433–1449. doi:10.1148/rg.295095034
39. Liu Y, Yang K, Cheng L, et al. PEGylated FePt@Fe_2O_3 core-shell magnetic nanoparticles: potential theranostic applications and *in vivo* toxicity studies. *Nanomedicine*. 2013;9(7):1077–1088. doi:10.1016/j.nano.2013.04.010
40. Passemard S, Staedler D, Učňová L, et al. Convenient synthesis of heterobifunctional poly(ethylene glycol) suitable for the functionalization of iron oxide nanoparticles for biomedical applications. *Bioorg Med Chem Lett*. 2013;23(17):5006–5010. doi:10.1016/j.bmcl.2013.06.037
41. Laurent S, Forge D, Port M, et al. Magnetic iron oxide nanoparticles: synthesis, stabilization, vectorization, physicochemical characterizations, and biological applications. *Chem Rev*. 2008;39(35):2064–2110. doi:10.1021/cr068445e
42. Shahnaz G, Kremser C, Reinisch A, et al. Efficient MRI labeling of endothelial progenitor cells: design of thiolated surface stabilized superparamagnetic iron oxide nanoparticles. *Eur J Pharm Biopharm*. 2013;85(3 Pt A):346–355. doi:10.1016/j.ejpb.2013.02.010
43. Alam MH, He T, Auger D, et al. Validation of T2* in-line analysis for tissue iron quantification at 1.5 T. *J Cardiov Magn Reson*. 2016;18(1):1–7. doi:10.1186/s12968-016-0243-4
44. Camargo GC, Rothstein T, Junqueira FP, et al. Comparison of myocardial T1 and T2 values in 3 T with T2* in 1.5 T in patients with iron overload and controls. *Int J Hematol*. 2016;103(5):530–536. doi:10.1007/s12185-016-1950-1
45. Van Zijl PC, Artemov D, Chan KW, et al. Use of non-labeled sugars and detection by MRI for assessing tissue perfusion and metabolism. U.S. Patent 9,180,211. 2015 November 10.
46. Reynolds PR, Larkman DJ, Haskard DO, et al. Detection of vascular expression of E-selectin in vivo with MR imaging. *Radiology*. 2006;241(2):469–476. doi:10.1148/radiol.2413051535
47. Sakhalkar H, Dalal M, Salem A, et al. Leukocyte-inspired biodegradable particles that selectively and avidly adhere to inflamed endothelium *in vitro* and *in vivo*. *Proc Natl Acad Sci USA*. 2003;100(26):15895–15900. doi:10.1073/pnas.2631433100
48. Boutry S, Laurent S, Elst L, Muller R. Specific E-selectin targeting with a superparamagnetic MRI contrast agent. *Contrast Media Mol I*. 2006;1(1):15–22. doi:10.1002/cmmi.87
49. McLachlan S, Morris M, Lucas M, et al. Phase I clinical evaluation of a new iron oxide MR contrast agent. *J Magn Reson Imaging*. 1994;4(3):301–307. doi:10.1002/jmri.1880040313
50. Weissleder R, Elizondo G, Wittenberg J, Rabito CA, Bengele HH, Josephson L. Ultrasmall superparamagnetic iron oxide: characterization of a new class of contrast agents for MR imaging. *Radiology*. 1990;175(2):489–493. doi:10.1148/radiology.175.2.\2326474